Control of Nonprehensile Rolling Manipulation: Balancing a Disk on a Disk

Ji-Chul Ryu, *Member, IEEE,* Fabio Ruggiero, *Member, IEEE,* and Kevin M. Lynch *Fellow, IEEE*

Abstract—This paper presents feedback stabilization control of a rolling manipulation system called the disk-on-disk. The system consists of two disks in which the upper disk (object) is free to roll on the lower disk (hand) under the influence of gravity. The goal is to stabilize the object at the unstable upright position directly above the hand. We show that it is possible to stabilize the object at the upright position while the hand or object rotates to a specific orientation or spins at a constant velocity. We use full-state feedback linearization to derive control laws. We present simulation as well as experimental results demonstrating the controllers.

Index Terms—rolling manipulation, nonprehensile manipulation, feedback linearization control, disk-on-disk.

I. INTRODUCTION

NONPREHENSILE manipulation primitives such as rolling, sliding, pushing, and throwing are commonly used by humans but usually avoided by robots, who seem to prefer grasping. Dynamic nonprehensile manipulation can raise challenges in high-speed sensing and control, as the manipulated object moves relative to the manipulator throughout the process. An advantage, however, is that dynamics can be exploited to allow the robot to create and control object motions that would otherwise be impossible. Examples include throwing an object outside the kinematic workspace of the robot and using rolling to control more object degrees of freedom than the robot has actuators [1]–[4].

Our long-term goal is to develop a unified framework for planning and control of dynamic robotic manipulation. A typical manipulation plan consists of a sequence of manipulation primitives (such as grasping, rolling, pushing, throwing, etc.), with each primitive equipped with its own motion planner and feedback controller. The primitive under study in this paper is nonprehensile rolling manipulation, where a single object rolls on the surface of a controlled manipulator. Problems of interest include planning the motion of the manipulator to achieve the desired rolling motion of the object (e.g., [2], [5]) and feedback control to stabilize the desired trajectory.

In this paper we study feedback stabilization of a canonical rolling problem: balancing a disk-shaped object on top of a disk-shaped manipulator (referred to as the hand) in a vertical plane. The balancing task is further extended to more

J. Ryu and K. M. Lynch are with the Department of Mechanical Engineering, Northwestern University, Evanston, IL, 60208, USA. K. M. Lynch is also affiliated with the Northwestern Institute on Complex Systems. email: {jcryu, kmlynch}@northwestern.edu. Fabio Ruggiero is with the PRISMA Lab, Dipartimento di Ingegneria Elettrica e Tecnologie dell'Informazione, Università degli Studi di Napoli Federico II, via Claudio 21, 80125, Naples, Italy, fabio.ruggiero@unina.it. Portions of this work were presented at IEEE ICRA 2012.

difficult problems of stabilization at the upright position while the hand or object (i) rotates to a specific orientation or (ii) spins at a constant velocity. We constrain the motion of the circular hand to rotation about its center. We derive control laws that stabilize the object to the balanced position under the kinematic assumption of rolling at all times. The basin of attraction is reduced when the contact is modeled using Coulomb friction, but it is still large with large friction coefficients. The effectiveness of the controllers has been verified in experiments.

This paper represents a first step toward control for general nonprehensile rolling manipulation by providing theoretical and experimental solutions for the canonical problem of a disk rolling on a disk.

A. Related Work

Several examples of control of rolling have been studied in the literature. Among them is the ball and beam system in which a ball rolls with one degree of freedom along a linear beam. The beam rotates in a vertical plane so the ball rolls under the influence of gravity. To solve the stabilization problem, approximate input-output linearization is used in [6], where the original equations of motion are approximated by a simplified nonlinear model such that the model becomes exact input-output linearizable. In [7], global asymptotic stability is achieved by a saturation control law which uses state-dependent saturation levels. A sliding mode controller that is robust to parameter uncertainty is also proposed in [8].

Another related problem is a ball rolling on a plate. It is shown in [9] that an admissible path between any two configurations exists and motion planning algorithms are provided in [9], [10]. The control inputs are the angular velocities of the ball, and these inputs can be generated by driving mechanisms inside the ball such as a small wheeled car [11] or rotors [12]. Motion of the ball can also be created by sandwiching the ball between the lower plate and an upper plate and controlling the motion of the upper plate, and controllers have been developed for this system using time-state control [13] and iterative feedback control [14]. Another variant of the ball-plate system is presented in [15] in which the ball rolls freely on a plate which rotates about its two planar axes. Balancing control is achieved using a linearized model of the dynamics.

The roles of the shape and motion of the manipulator in determining the motion of the rolling object were studied in the context of the "butterfly" contact juggling trick in [5]. No analysis is provided of feedback stabilization of rolling trajectories or balanced configurations, however. Inspired by

this work, two-phase stabilization control for the butterfly system is addressed in [16] with an energy-based "swing-up" controller followed by an LQR controller based on linear approximation. The rolling ball is modeled as a simple sliding point mass, and no experimental validation of the controller is provided.

This paper extends our previous work [17] in which we solve a feedback control problem of balancing the object at the unstable upright position. Compared to this balancing-only problem, we study in this paper more difficult problems of balancing with the hand or object at a desired angle or angular velocity.

B. Paper Outline

In Section II, the kinematic and dynamic equations of the disk-on-disk system are derived. In Section III, stabilizing controllers that achieve our control objectives are designed based on full-state feedback linearization. Simulation results are provided in Section IV. The experimental setup and experimental results are presented in Sections V and VI, respectively. Concluding remarks with future research directions are given in Section VII.

II. DYNAMICS OF THE DISK-ON-DISK

In this section, we derive the kinematic and dynamic equations of a smooth planar object rolling on a smooth, motion-controlled planar manipulator, referred to as the "hand." We then restrict to the special case of the disk-on-disk in Section II-C.

We define a coordinate frame u_h-v_h attached to the hand and let $p_h \in \mathbb{R}^2$ be the position and θ_h be the orientation of the frame in a world reference frame x-y (Fig. 1). The position and orientation of the frame u_o-v_o, which is attached to the center of mass of the object, are given by $p_o \in \mathbb{R}^2$ and θ_o, respectively.

The curve of the hand is parameterized by an arclength parameter $s_h \in \mathbb{R}$, and the shape of the hand is given by $c_h(s_h) \in \mathbb{R}^2$ in the u_h-v_h frame. The parameter s_h increases counterclockwise along the hand. The object is parameterized by an arclength parameter s_o, where s_o increases clockwise, and the object shape in the u_o-v_o frame is given by $c_o(s_o) \in \mathbb{R}^2$. With this choice, the pure rolling assumption yields $\dot{s}_h = \dot{s}_o$. By an appropriate choice of the location of $s_o = 0$, we have $s_h = s_o$ at all times during rolling. For this reason, we specify the contact location by s_h only and do not refer to s_o.

Assuming the hand and object maintain rolling contact at all times, the system's configuration is fully specified by $q = [p_h^T, \theta_h, s_h]^T$.

A. Kinematic Equations

When we derive the rolling dynamics, it will be necessary to reconstruct the object's position p_o and orientation θ_o from the minimal configuration representation $q = [p_h^T, \theta_h, s_h]^T$. This subsection provides the necessary equations.

At a contact point $c_h(s_h) = [u_h(s_h), v_h(s_h)]^T$, the tangent vector is expressed as $t = c_h' = [u_h', v_h']^T$ at an angle $\phi_h =$
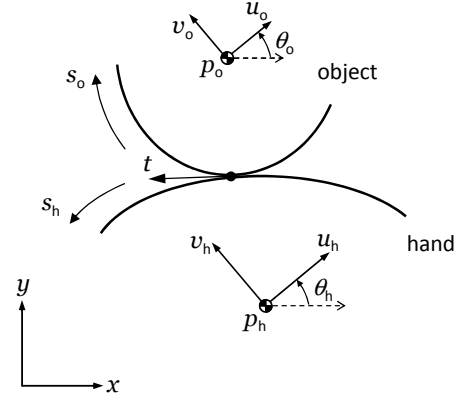

Fig. 1. A schematic of a general planar rolling manipulation system. The u_h-v_h frame is attached to the hand and θ_h denotes its orientation with respect to the x-y world frame. Similarly, the u_o-v_o frame is attached to the object and θ_o denotes the frame's orientation.

atan2(v_h', u_h') in the u_h-v_h frame, where the symbol $\prime$ indicates a derivative with respect to the arclength parameter. Using the property $\|\frac{dc_h}{ds_h}\| = 1$ of arclength parameterizations, the signed curvature of the hand can be written as

$$\kappa_h(s_h) = \frac{d\phi_h}{ds_h} = u_h'(s_h)v_h''(s_h) - u_h''(s_h)v_h'(s_h), \quad (1)$$

where $\kappa_h > 0$ means the hand is convex at the contact point. Similarly, the signed curvature of the object is given by

$$\kappa_o(s_h) = \frac{d\phi_o}{ds_h} = u_o'(s_h)v_o''(s_h) - u_o''(s_h)v_o'(s_h), \quad (2)$$

where $\phi_o = $ atan2(v_o', u_o'). Due to the opposite sense of the parameterization, $\kappa_o < 0$ indicates convexity. The relative curvature at s_h is

$$\kappa_r(s_h) = \kappa_h(s_h) - \kappa_o(s_h), \quad (3)$$

where $\kappa_r > 0$ guarantees a single contact point locally.

The angle of the tangent vector measured in the world reference frame is written as

$$\theta_h + \phi_h = \theta_o + \phi_o$$

yielding

$$\theta_o = \theta_h + \text{atan2}(v_h', u_h') - \text{atan2}(v_o', u_o'), \quad (4)$$
$$\dot{\theta}_o = \dot{\theta}_h + \dot{s}_h\kappa_r(s_h), \quad (5)$$
$$\ddot{\theta}_o = \ddot{\theta}_h + \ddot{s}_h\kappa_r(s_h) + \dot{s}_h^2\kappa_r'(s_h). \quad (6)$$

To determine the dependence of p_o and its derivatives on q and its derivatives, we start with the condition that the contact point on the hand and object are coincident,

$$p_h + R(\theta_h)c_h(s_h) = p_o + R(\theta_o)c_o(s_h), \quad (7)$$

where the rotation matrix $R(\theta) \in SO(2)$ is given by

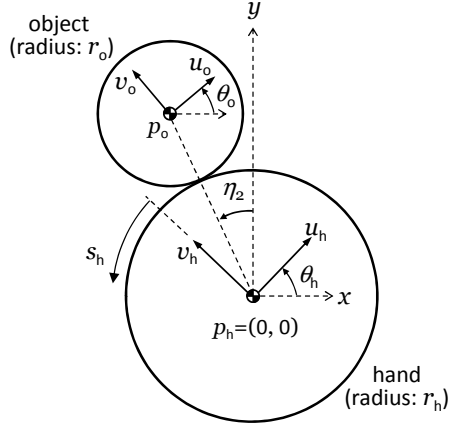$$R(\theta) = \begin{bmatrix} \cos\theta & -\sin\theta \\ \sin\theta & \cos\theta \end{bmatrix}.$$

Fig. 2. A schematic of the disk-on-disk system. Both the hand and object are circular disks, and the hand is constrained to rotate about its center at the origin of the x-y world frame. The angle η_2 is measured counterclockwise from the y-axis of the world frame to the center of the object.

Noticing that $\frac{d}{dt}R(\theta) = \dot{\theta}R(\theta + \frac{\pi}{2})$ and plugging in (5), we obtain

$$p_o = p_h + R(\theta_h)c_h - R(\theta_o)c_o, \tag{8}$$
$$\dot{p}_o = \dot{p}_h + \left(R(\theta_h + \tfrac{\pi}{2})c_h - R(\theta_o + \tfrac{\pi}{2})c_o\right)\dot{\theta}_h + \left(R(\theta_h)c_h' - \kappa_r R(\theta_o + \tfrac{\pi}{2})c_o - R(\theta_o)c_o'\right)\dot{s}_h. \tag{9}$$

The expression for $\ddot{p}_o$ is obtained by differentiating (9) with respect to time and is omitted due to length.

B. Dynamic Equations

The dynamic equations are derived from Lagrange's equations

$$\frac{d}{dt}\frac{\partial L}{\partial \dot{q}} - \frac{\partial L}{\partial q} = \tau \tag{10}$$

with Lagrangian $L = K - U$ and the vector of generalized forces τ, where the kinetic energy K and potential energy U are given by

$$K = \frac{1}{2}\left(m_h \dot{p}_h^T \dot{p}_h + I_h \dot{\theta}_h^2 + m_o \dot{p}_o^T \dot{p}_o + I_o \dot{\theta}_o^2\right), \tag{11}$$

$$U = g(m_h p_h^T + m_o p_o^T)\begin{bmatrix}0\\1\end{bmatrix}, \tag{12}$$

where m_h, I_h and m_o, I_o are the mass and moment of inertia of the hand and object, respectively, and g is the gravitational acceleration. Inserting the expressions (4), (5), (8), and (9) into Lagrange's equations (10) yields the dynamic equations.

C. The Disk-on-Disk System

We now derive the dynamics for the disk-on-disk shown in Fig. 2. The radii of the hand and object disks are r_h and r_o, respectively, and the hand is constrained to rotation only, i.e., $p_h = 0$.

Given a contact point expressed in the u_h-v_h and the u_o-v_o frames respectively as

$$c_h(s_h) = \begin{bmatrix}-r_h \sin(s_h/r_h)\\ r_h \cos(s_h/r_h)\end{bmatrix}, \tag{13}$$

$$c_o(s_h) = \begin{bmatrix}-r_o \sin(s_h/r_o)\\ -r_o \cos(s_h/r_o)\end{bmatrix}, \tag{14}$$

from (1)–(3) we obtain the constant signed and relative curvatures

$$\kappa_h = 1/r_h, \quad \kappa_o = -1/r_o, \quad \kappa_r = \frac{r_h + r_o}{r_h r_o}. \tag{15}$$

Consequently, using (4)–(6), we obtain

$$\theta_o = \theta_h + \kappa_r s_h, \tag{16}$$
$$\dot{\theta}_o = \dot{\theta}_h + \kappa_r \dot{s}_h, \tag{17}$$
$$\ddot{\theta}_o = \ddot{\theta}_h + \kappa_r \ddot{s}_h. \tag{18}$$

Substituting (13) and (14) into (8) and (9) and rearranging, we have

$$p_o = \begin{bmatrix}-(r_h + r_o)\sin(\theta_h + s_h/r_h)\\ (r_h + r_o)\cos(\theta_h + s_h/r_h)\end{bmatrix}, \tag{19}$$

$$\dot{p}_o = \begin{bmatrix}-(r_h + r_o)\cos(\theta_h + s_h/r_h)(\dot{\theta}_h + \dot{s}_h/r_h)\\ -(r_h + r_o)\sin(\theta_h + s_h/r_h)(\dot{\theta}_h + \dot{s}_h/r_h)\end{bmatrix}, \tag{20}$$

$$\ddot{p}_o = \begin{bmatrix}-(r_h + r_o)\cos(\theta_h + s_h/r_h)(\ddot{\theta}_h + \ddot{s}_h/r_h)\\ +(r_h + r_o)\sin(\theta_h + s_h/r_h)(\dot{\theta}_h + \dot{s}_h/r_h)^2\\ -(r_h + r_o)\sin(\theta_h + s_h/r_h)(\ddot{\theta}_h + \ddot{s}_h/r_h)\\ -(r_h + r_o)\cos(\theta_h + s_h/r_h)(\dot{\theta}_h + \dot{s}_h/r_h)^2\end{bmatrix}. \tag{21}$$

Inserting these expressions into Lagrange's equations, we solve for the dynamics

$$m_{11}\ddot{\theta}_h + m_{12}\ddot{s}_h + h_1(q) = \tau_h, \tag{22a}$$
$$m_{21}\ddot{\theta}_h + m_{22}\ddot{s}_h + h_2(q) = 0, \tag{22b}$$

where

$$m_{11} = I_h + I_o + m_o(r_h + r_o)^2, \tag{23}$$
$$m_{12} = m_{21} = m_o(r_h + r_o)^2/r_h + I_o\kappa_r, \tag{24}$$
$$m_{22} = \kappa_r^2(m_o r_o^2 + I_o), \tag{25}$$
$$h_1(q) = -m_o g(r_h + r_o)\sin(\theta_h + s_h/r_h), \tag{26}$$
$$h_2(q) = -m_o g r_o \kappa_r \sin(\theta_h + s_h/r_h). \tag{27}$$

In our experimental implementation, we use a highly-geared harmonic drive DC motor to drive the hand. For this reason, it is more convenient to consider the hand's angular acceleration (created by a low-level acceleration controller) as the system input rather than the torque τ_h in (22a). Defining this new acceleration control as $v = \ddot{\theta}_h$ and substituting into (22b), we rewrite the dynamics as

$$\ddot{\theta}_h = v, \tag{28a}$$
$$\ddot{s}_h = -\frac{1}{m_{22}}(m_{12}v + h_2(q)). \tag{28b}$$

By plugging (28) into (22a), the relationship between the hand torque τ_h and the new input v is found to be

$$\tau_h = \left(m_{11} - \frac{m_{12}^2}{m_{22}}\right)v - \frac{m_{12}}{m_{22}}h_2 + h_1. \tag{29}$$

D. Friction Constraints

The previous derivations are predicated on the assumption that $s_\text{h} = s_\text{o}$ at all times, i.e., rolling is guaranteed. For some states and controls, however, this assumption of rolling may require the hand to "pull" on the object, i.e., it requires negative normal force f_n, which is not physically possible. In others the magnitude of the required friction force f_f may be greater than μf_n (μ is the Coulomb friction coefficient), which is also not possible and implies slip would occur. The conditions the contact forces must satisfy can be expressed abstractly as constraints on the state $(q, \dot{q})$ and control v:

$$F_\text{n}(q, \dot{q}, v) \geq 0, \tag{30}$$
$$F_\text{f}(q, \dot{q}, v) \leq \mu, \tag{31}$$

where the first condition represents the normal force constraint and the second the friction force constraint. The larger the friction coefficient μ, the larger the volume of the state-control space that satisfies the friction conditions for rolling. Outside of this volume, the object slips or falls from the hand. These constraints are not explicitly incorporated in the design of the control laws, but their effects are considered in the simulation studies.

III. STABILIZATION CONTROL

In this section we propose a controller that performs the following control tasks: (i) balancing of the object at the upright position at a desired orientation and (ii) balancing of the object at the upright position while spinning at a constant velocity.

The controller is based on full-state feedback linearization and it is able to complete both tasks using the same framework with a slight difference in the choice of the change of coordinates.

A. Balancing with the Hand or Object at a Desired Angle

In this subsection, we propose a controller that rotates the hand or object disk to a specific angular position while balancing the object at the upright position. We present this controller to control the hand angular position, but object angular position control is also possible under the same framework and will be explained later in this subsection.

The system described by (28) can be expressed in state-space form with the state variable $z = [\theta_\text{h}, \dot{\theta}_\text{h}, s_\text{h}, \dot{s}_\text{h}]^T$ as

$$\dot{z}_1 = z_2, \tag{32a}$$
$$\dot{z}_2 = v, \tag{32b}$$
$$\dot{z}_3 = z_4, \tag{32c}$$
$$\dot{z}_4 = -\frac{h_2(z)}{m_{22}} - \frac{m_{12}}{m_{22}} v. \tag{32d}$$

The task in this subsection will be completed by driving both velocities z_2 and z_4 to zero and z_1 to a specific angular position with the center of mass of the object directly above the center of the hand (the balanced position). Because the states z_1 and z_3 couple to determine the location of the center

of mass of the object, we introduce the following change of coordinates:

$$\eta_1 = m_{22} \dot{s}_\text{h} + m_{12} \dot{\theta}_\text{h}, \tag{33a}$$
$$\eta_2 = \theta_\text{h} + s_\text{h}/r_\text{h}, \tag{33b}$$
$$\delta = \theta_\text{h} - \theta_\text{h}^*, \tag{33c}$$
$$\xi = \dot{\theta}_\text{h}, \tag{33d}$$

where θ_h^* represents a target angular position of the hand. The new state η_2 represents the angle to the center of the object measured counterclockwise with respect to the y-axis of the world frame (Fig. 2). Hence, $\eta_2 = 0$ implies the object is at the upright balanced position. The states η_1 and ξ span the original velocity space z_2-z_4. The job of the controller is now to stabilize all the states to zero.

The dynamic model is now written as

$$\dot{\eta}_1 = \sigma_1 \sin \eta_2, \tag{34a}$$
$$\dot{\eta}_2 = \sigma_2 \eta_1 + \sigma_3 \xi, \tag{34b}$$
$$\dot{\delta} = \xi, \tag{34c}$$
$$\dot{\xi} = v. \tag{34d}$$

where $\sigma_1 \equiv m_\text{o} g (r_\text{h} + r_\text{o})/r_\text{h}$, $\sigma_2 \equiv 1/(r_\text{h} m_{22})$, and $\sigma_3 \equiv 1 - m_{12}/(r_\text{h} m_{22})$.

This system is full-state feedback linearizable [18, chap 4] if there exists a linearizing output h satisfying

$$\nabla h \, \text{ad}_f^i g = 0, \quad i = \{0, 1, 2\}, \tag{35a}$$
$$\nabla h \, \text{ad}_f^2 g \neq 0, \tag{35b}$$

where $\text{ad}_f g$ denotes the Lie bracket defined by $\text{ad}_f g = \nabla g f - \nabla f g$, $f = [\sigma_1 \sin \eta_2, \sigma_2 \eta_1 + \sigma_3 \xi, \xi, 0]^T$, and $g = [0, 0, 0, 1]^T$. The full-state feedback linearization allows us to transform the nonlinear system (34) to a linear one and the derivatives of the output h correspond to the states of the transformed linear system. We solve (35) for the output h as $h = \eta_2 - \sigma_3 \delta$.

Taking derivatives of h until the input v appears yields

$$\dot{h} = \dot{\eta}_2 - \sigma_3 \dot{\delta}$$
$$= \sigma_2 \eta_1, \tag{36}$$
$$\ddot{h} = \sigma_2 \sigma_1 \sin \eta_2, \tag{37}$$
$$\dddot{h} = \sigma_2 \sigma_1 \cos \eta_2 (\sigma_2 \eta_1 + \sigma_3 \xi), \tag{38}$$
$$h^{(4)} = \beta(x) + \gamma(x) v, \tag{39}$$

where, with $x = [\eta_1, \eta_2, \delta, \xi]^T$,

$$\beta(x) = \sigma_1 \sigma_2 \sin \eta_2 \left(\sigma_1 \sigma_2 \cos \eta_2 - (\sigma_2 \eta_1 + \sigma_3 \xi)^2 \right), \tag{40}$$
$$\gamma(x) = \sigma_1 \sigma_2 \sigma_3 \cos \eta_2. \tag{41}$$

By introducing the input transformation

$$v = \frac{1}{\gamma(x)} (u - \beta(x)), \tag{42}$$

the nonlinear system (34) results in a linear system (quadruple integrator) given by

$$\dot{y}_1 = y_2,$$
$$\dot{y}_2 = y_3,$$
$$\dot{y}_3 = y_4, \tag{43}$$
$$\dot{y}_4 = u,$$

where $y = [y_1, y_2, y_3, y_4]^T = [h, \dot{h}, \ddot{h}, \dddot{h}]^T$. If we differentiate the output r times until the input appears, the number r is called the relative degree of the system. In order for a system to be full-state feedback linearizable, the relative degree must be equal to the order of the system itself. As shown in (39), the relative degree of the system is four ensuring full-state feedback linearization with no internal dynamics.

The new control input u can be easily designed as

$$u = -k_1 y_4 - k_2 y_3 - k_3 y_2 - k_4 y_1, \tag{44}$$

where k_i are positive control gains. This feedback control law gives a characteristic equation of

$$s^4 + k_1 s^3 + k_2 s^2 + k_3 s + k_4 = 0, \tag{45}$$

where the k_i are determined so that the roots of the characteristic equation lie in the left half plane. This choice of k_i stabilizes the origin $y = 0$ and consequently the origin of the original space, $x = [\eta_1, \eta_2, \delta, \xi]^T = 0$.

The coordinate transformation (diffeomorphism) described by $y = T(x)$ is valid in the region $\Omega = \{|\eta_2| < \frac{\pi}{2}\}$ since the input transformation (42) is not defined when $\gamma(x) = 0$, i.e., $\cos \eta_2 = 0$. Note that the basin of attraction is practically global since, with no bound on other states, the region Ω determined by η_2 covers all physically possible configurations (outside of this region, the object must fall from the hand).

Remark 3.1: Control of the object's angular position θ_o is also possible by selecting the output $h = \eta_2 - \sigma_3' \delta$ with the state $\delta = \theta_o - \theta_o^*$, where $\sigma_3' = \sigma_3/(1 - \frac{\kappa_r m_{12}}{m_{22}})$. Then we obtain the first derivative of δ, using (17), (33a), and (33d)

$$\dot{\delta} = \dot{\theta}_o = \dot{\theta}_h + \kappa_r \dot{s}_h$$
$$= \frac{\kappa_r}{m_{22}} \eta_1 + \left(1 - \frac{\kappa_r m_{12}}{m_{22}}\right) \xi. \tag{46}$$

As a result, the derivative of h is given by

$$\dot{h} = \dot{\eta}_2 - \sigma_3' \dot{\delta},$$
$$= \sigma_2' \eta_1, \tag{47}$$

where $\sigma_2' = \sigma_2 - \sigma_3' \kappa_r / m_{22}$. The output h and its derivatives then have the same form as the hand position control. Therefore, the same control law (42) can be applied to object angle control with the constants δ_2' and δ_3' replacing δ_2 and δ_3, respectively.

B. Balancing with Angular Velocity Control

In this subsection, the control objective of spinning of the hand or object at a constant velocity while balancing the object at the upright position is achieved by the same framework of the feedback linearization controller in the previous subsection. To this end, we modify the state δ as $\delta = \theta_h - \dot{\theta}_h^* t$, where t denotes time and $\dot{\theta}_h^*$ the target hand velocity, yielding the following dynamic model

$$\dot{\eta}_1 = \sigma_1 \sin \eta_2, \tag{48a}$$
$$\dot{\eta}_2 = \sigma_2 \eta_1 + \sigma_3 \xi, \tag{48b}$$
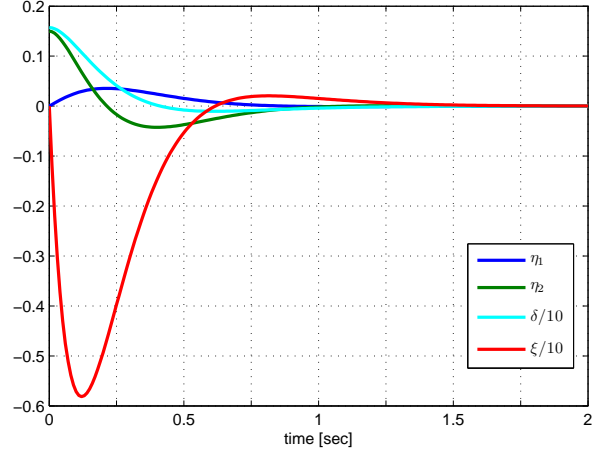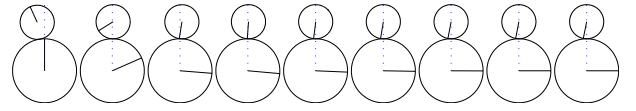$$\dot{\delta} = \xi - \dot{\theta}_h^*, \tag{48c}$$
$$\dot{\xi} = v. \tag{48d}$$

Fig. 3. Simulation results showing η_1, η_2, δ, and ξ converging to zero for balancing with angular position control. The quantities $\frac{1}{10}\delta$ and $\frac{1}{10}\xi$ are plotted instead of δ and ξ so they can be shown on the same scale as η_1 and η_2. The icons at top show the configurations of the disks every 0.25 seconds.

This choice of δ could be interpreted as hand position control with changing target position at a constant rate of $\dot{\theta}_h^*$.

The relative degree of the new system is still four, so the same form of the control law given in (42) and (44) can be used with $y_2 = \dot{h} = \sigma_2 \eta_1 + \sigma_3 \dot{\theta}_h^*$. However, the convergence of the feedback linearized system (43) to the origin now corresponds to that of the original system (48) to $(\eta_1, \eta_2, \delta, \xi) = (-\frac{\sigma_3}{\sigma_2} \dot{\theta}_h^*, 0, 0, \dot{\theta}_h^*)$.

The object velocity in steady state relates to the hand (target) velocity $\dot{\theta}_h^*$ such that

$$\dot{\theta}_o^* = -\frac{r_h}{r_o} \dot{\theta}_h^* \tag{49}$$

from using the time derivative of (33b) with $\dot{\eta}_2 = 0$ (in steady state) and (17). The control of the object velocity can be achieved using this relationship.

IV. SIMULATION RESULTS

Simulation results for the two control tasks are shown in this section. The values of parameters used in the simulation are the actual values of the disk-on-disk system constructed for experiment in Section V-A: $m_o = 0.142$ kg, $r_o = 0.08$ m, $I_o = 0.4544 \times 10^{-3}$ kg·m^2, $r_h = 0.15$ m, and $g = 9.62$ m/s^2 (98.2 % of full gravity). All angles are measured in radians, and all units are SI unless otherwise noted.

A. Balancing with the Hand or Object at a Desired Angle

For the simulation, we choose the control gains (k_1, k_2, k_3, k_4) such that the all roots of the characteristic equation (45) lie at -6 (in the left half plane), which yields $(k_1, k_2, k_3, k_4) = (24, 216, 864, 1296)$. Given the initial
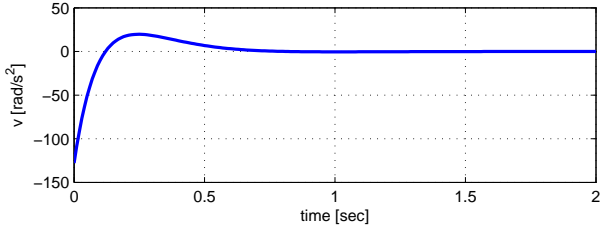
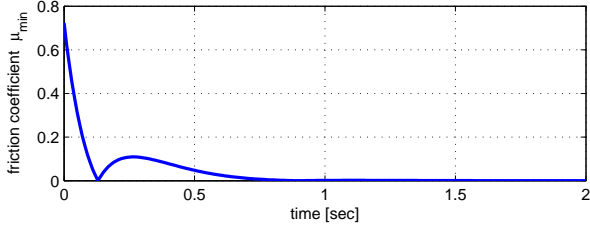Fig. 4. Simulation result of the acceleration input v.

Fig. 5. A plot of the minimum friction coefficient required to prevent slipping at the contact during balancing. The friction force changes sign at approximately $t = 0.13$ s.

Fig. 6. Simulation results showing η_1, η_2, δ, and ξ for balancing with angular velocity control.

condition $\eta_2(0) = 0.15$ and $\theta_{\mathrm{h}}(0) = 0$, the corresponding initial conditions of θ_{o} and s_{h} are calculated as $\theta_{\mathrm{o}}(0) = 0.431$ and $s_{\mathrm{h}}(0) = 0.023$ from (16) and (33b). The disks are initially at rest at the initial configuration, giving $\eta_1(0) = 0$ and $\xi(0) = 0$. The target hand position is $\theta_{\mathrm{h}}^* = -\frac{\pi}{2}$ yielding $\delta(0) = \frac{\pi}{2}$.

As shown in Fig. 3, all the state variables η_1, η_2, δ, and ξ converge to zero, which physically means that the object stabilizes to the position directly above the hand with its angular velocity converging to zero while the angular position of the hand converges to the target position of $-\frac{\pi}{2}$. The icons above Fig. 3 show the configurations of the two disks every 0.25 seconds and they also show the positions of the hand at $-\frac{\pi}{2}$ in the steady state. Fig. 4 shows the input angular acceleration v (42) to the hand.

The necessary friction coefficient μ to ensure rolling is calculated as

$$\mu \geq \frac{|f_{\mathrm{f}}|}{f_{\mathrm{n}}},$$

where f_{f} represents the friction force and f_{n} the normal force at a contact point. These contact forces acting on the object can be determined from the object's acceleration added with the force to counteract gravity such that

$$f_{\mathrm{n}} = m_{\mathrm{o}}(\ddot{y}_{\mathrm{o}} + g)\cos\eta_2 - m_{\mathrm{o}}\ddot{x}_{\mathrm{o}}\sin\eta_2, \qquad (50)$$

$$f_{\mathrm{f}} = m_{\mathrm{o}}(\ddot{y}_{\mathrm{o}} + g)\sin\eta_2 + m_{\mathrm{o}}\ddot{x}_{\mathrm{o}}\cos\eta_2. \qquad (51)$$

In turn, inserting (21) with $\eta_2 = \theta_{\mathrm{h}} + s_{\mathrm{h}}/r_{\mathrm{h}}$ we have

$$f_{\mathrm{n}} = -m_{\mathrm{o}}(r_{\mathrm{h}} + r_{\mathrm{o}})(\sigma_2\eta_1 + \sigma_3\xi)^2 + m_{\mathrm{o}}g\cos\eta_2, \qquad (52)$$

$$f_{\mathrm{f}} = -m_{\mathrm{o}}(r_{\mathrm{h}} + r_{\mathrm{o}})(\sigma_2\sigma_1\sin\eta_2 + \sigma_3 v) + m_{\mathrm{o}}g\sin\eta_2. \qquad (53)$$

As noted earlier, the contact forces f_{n} and f_{f} are a function of the state (η_1, η_2, ξ) and control v. Substituting the simulation results into these contact force expressions, Fig. 5 plots the minimum friction coefficient μ needed to ensure rolling as a
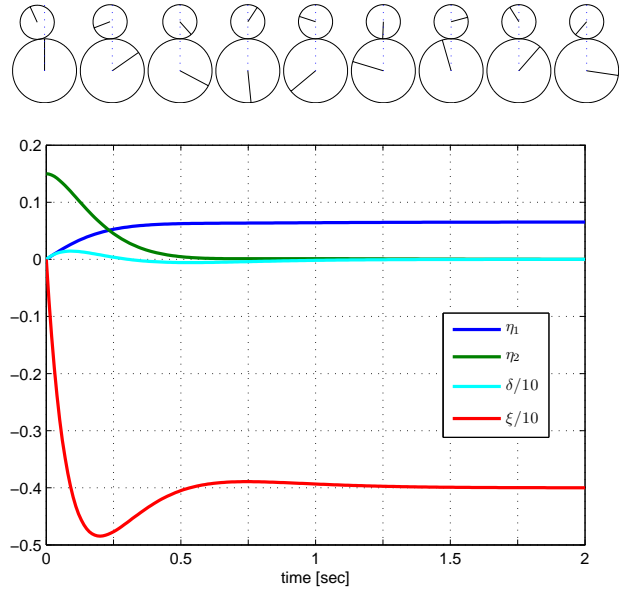
function of time. At the beginning of the run, when the object is left of center, the large control acceleration v requires a large friction coefficient to prevent slipping. As the object becomes balanced above the hand, the friction coefficient required for rolling drops to zero.

B. Balancing with Angular Velocity Control

For this simulation, we again choose the control gains $(k_1, k_2, k_3, k_4) = (24, 216, 864, 1296)$. The target hand velocity is set at -4 rad/s. The object also starts from rest at the initial condition $\eta_2(0) = 0.15$.

As shown in Fig. 6, the state δ converges to zero, i.e., the angular position of the hand converges to the target velocity of -4 rad/s. The convergence of the hand velocity to -4 rad/s is more directly observed with the state ξ. The state η_2 also converges to zero indicating that the center of the object converges to directly above the hand. In fact, $\eta_1 = -\frac{\sigma_3}{\sigma_2}\xi$ in the steady state, which is obtained from (38) by substituting $\dddot{h} = 0$. The icons above the figure show that the hand and object keep rotating.

Remark 4.1: We might ask whether it is possible to balance the object at a position not directly above the center of the hand. This is not practically possible, as the vertical contact force needed to cancel gravity necessarily creates a moment about the object's center of mass. This means that the object (and the hand) must rotate at a constant angular acceleration, resulting in unbounded velocities. This can be seen in the governing equations (34) by plugging a constant value into η_2 and setting $\dot{\eta}_2 = 0$.
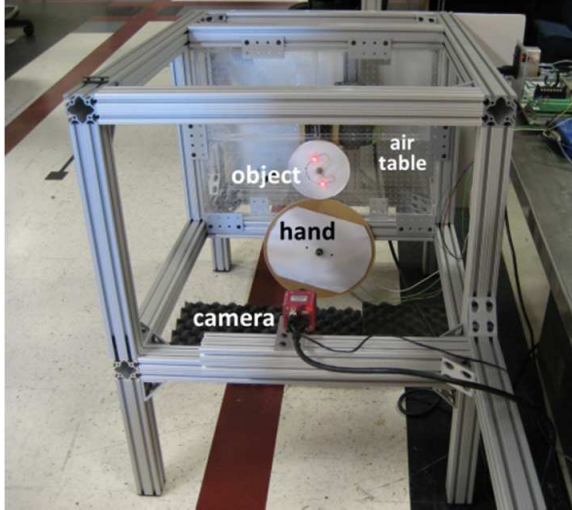
Fig. 7. The disk-on-disk experimental setup. The upper disk (object) rolls on the lower disk (hand). The hand is actuated by a harmonic drive DC motor. A high speed camera and vision system is used for visual feedback of the object. This snapshot was taken when the system was under control action.
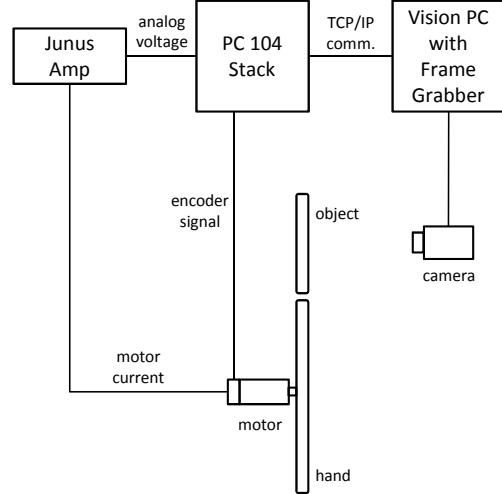

Fig. 8. Schematic of the experimental set-up showing signal paths with a side view of the hand and object. The actual disk-on-disk system is tilted $79.0°$ with respect to the horizontal plane.

V. EXPERIMENTAL SETUP

A. Hardware

Fig. 7 shows our disk-on-disk experimental setup. The hand is the lower disk, actuated by a harmonic drive DC motor (Harmonic Drive RH-8D 6006) equipped with a 50:1 harmonic drive gearhead and a 500 ppr quadrature encoder giving 100,000 counts per revolution at the output shaft. The object disk is free to roll on the hand. The commanded current input to the motor is provided through a motor amplifier (Copley Controls Junus 800-1468). The disk-on-disk system is mounted on an air table that provides frictionless support in a plane tilted $79.0°$ with respect to horizontal (98.2% of full gravity). Both hand and object are made of $1/4$ inch thick acrylic and the object is encircled by a rubber band to increase friction.

The hand control algorithm runs on a PC104 stack with a QNX real-time operating system (RTOS). In addition to the angular position data from the encoder of the hand, the controller utilizes the state of the object disk, which is determined using a high-speed vision system. The vision system, consisting of a PhotonFocus TrackCam camera, a Microenable III frame grabber, and a Windows PC, tracks two markers on the disk at 800 Hz, allowing estimation of the position and orientation of the disk at 800 Hz. The vision program, written in C++, sends the orientation of the disk to the controller PC104 stack via TCP/IP. The tracking markers may be high contrast passive markers (e.g., black on white) or active markers (LEDs in the current implementation).

B. Controller Implementation

The control algorithm is written in C++ and runs on the PC104 stack. Using the QNX RTOS, the control loop runs at 800 Hz in sync with the vision system. As the control law requires the angular velocity of each disk, we apply differencing plus low-pass filters to the encoder and vision data to estimate velocity.

Since our control law (42) generates acceleration commands v, we implement an additional acceleration control loop converting these controls to the motor current requested from the motor amplifier. This inner controller is written

$$i_{\text{com}} = i_{\text{ff}}(\dot{\theta}_{\text{h}}, v) + k_{\text{p}}(\theta_{\text{ref}} - \theta_{\text{h}}) + k_{\text{d}}(\dot{\theta}_{\text{ref}} - \dot{\theta}_{\text{h}}), \qquad (54)$$

where i_{com} is the commanded motor current, i_{ff} is a feedforward motor current based on the hand's angular velocity and requested acceleration, θ_{ref} and $\dot{\theta}_{\text{ref}}$ are the desired hand position and velocity obtained by integrating the acceleration command $v(t)$, and k_{p} and k_{d} are PD gains. The feedforward motor current is based on the simple model

$$(I_{\text{h}} + I_{\text{m}})\ddot{\theta}_{\text{h}} = k_{\text{m}}i - \mu_{\text{d}}\dot{\theta}_{\text{h}} - f_{\text{s}}\text{sgn}(\dot{\theta}_{\text{h}}), \qquad (55)$$

where I_{h} and I_{m} denote the inertia of the hand and the motor rotor, respectively, k_{m} is the motor constant, i is the motor current, μ_{d} is a viscous friction coefficient, f_{s} is the torque required to overcome friction from rest, and the function $\text{sgn}(\cdot)$ returns the sign of its argument. The inertia of the motor I_{m} is the reflected inertia due to the gearhead. We estimated the values of k_{m}, μ_{d}, and f_{s} in motor modeling experiments, and the feedforward current i_{ff} is calculated by substituting the commanded acceleration v and current hand velocity $\dot{\theta}_{\text{h}}$ into (55). After estimating the parameters of the feedforward model, the PD gains were tuned experimentally to reject modeling errors, yielding $(k_{\text{p}}, k_{\text{d}}) = (150, 0.9)$. Fig. 9 shows that the inner loop acceleration controller (54) provides satisfactory tracking of the commanded hand acceleration v.

VI. EXPERIMENTAL RESULTS

The video attachment shows experimental runs of the different controllers performed in a continuous series (This video can also be seen at https://vimeo.com/54405698). The initial
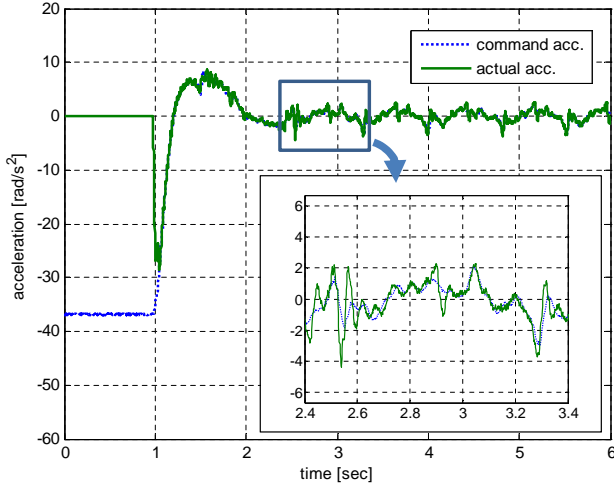
Fig. 9. Experimental result showing the command and actual accelerations of the hand for an experimental run. The actual acceleration follows the command acceleration satisfactorily. The control action starts at $t = 1.00$ s.
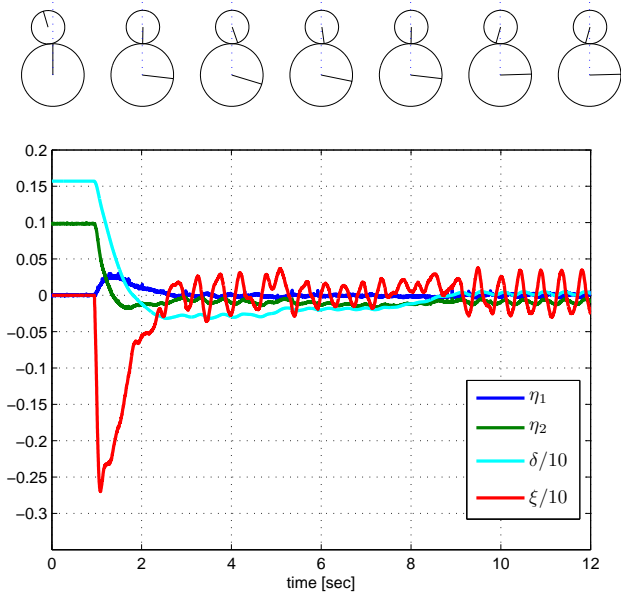

Fig. 10. Experimental result showing the state variables η_1, η_2, δ, and ξ for balancing with angular position control. The target angle of the hand is $-\frac{\pi}{2}$. The control action starts at $t = 0.95$ s. The icons at top show the configurations of the disks every 2 seconds.

conditions of each task do not correspond to the controlled initial conditions in the data presented below.

A. Balancing with the Hand or Object at a Desired Angle

The feedback linearization controller in this experiment was commanded to rotate the hand to negative 90 degrees while balancing the object to the upright position. Since feedback linearization-based controllers generally possess high sensitivity to parametric uncertainty or unmodeled dynamics, to enhance its robustness we added an additional term ρ using integral control [19, chap 12.4] to the control input (44) such
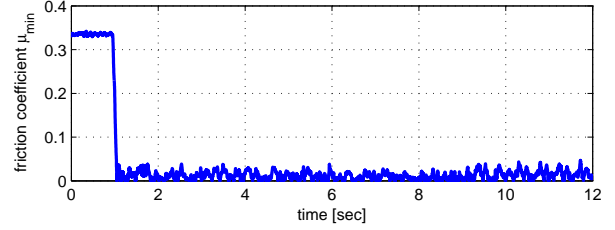

Fig. 11. A plot of the minimum friction coefficient required to prevent slipping at the contact during the experiment. This plot uses the experimental data of the states and control input to calculate the friction coefficient.

that

$$u = -k_1 y_4 - k_2 y_3 - k_3 y_2 - k_4 y_1 - k_5 \rho, \qquad (56)$$

where the variable ρ is integrating the position error, defined as $\dot{\rho} = \theta_\mathrm{h}^* - \theta_\mathrm{h}$. With this choice of ρ, stability is guaranteed locally near the equilibrium position, but the basin of attraction appears to be large enough for the given initial conditions. The same control gains of $(k_1, k_2, k_3, k_4) = (24, 216, 864, 1296)$ were used with $k_5 = 100$.

Fig. 10 shows the state variables $(\eta_1, \eta_2, \delta, \xi)$ for one experimental run. The initial condition of the experiment was set at $(\eta_1, \eta_2, \delta, \xi) = (0, 0.099, 1.57, 0)$, which means that initially both disks were at rest and the object disk was placed with its center of mass at an angle of 0.099 rad (5.67°) relative to the world y-axis. The object disk was kept at rest at the initial position using a small block until control action starts at $t = 0.95$ s.

After the hand angular position θ_h settles within the range of ± 5 % of the initial condition at $t = 8.90$ s, the RMS error of θ_h is 0.030 (1.719°) for the target hand position of $-\frac{\pi}{2}$. Similarly, after $t = 8.90$ s, the RMS errors of η_2, which is the angle to the center of the object with respect to the y-axis, is 0.0092 (0.527°) and the RMS errors of η_1 and ξ, which are related to the angular velocities of the object and hand, are 0.0015 and 0.2018, respectively. Due to the added integral action, the response of θ_h, which can be seen by the hand position error δ, shows a long settling time and overshoot during the transient period in Fig. 10.

We observed the appearance of small-amplitude limit cycles near the balanced configuration. That is because the simulation and experiment differ in a number of ways, including discrete-time implementation, approximate control of the motor acceleration, quantized position sensing, continuous small perturbations from the air table, etc.

Fig. 11 shows that the friction coefficient to prevent slipping is required to be greater than 0.34 for this experiment (at the beginning of the run). This plot uses the experimental data of the states and control input to calculate the required minimum friction coefficient using (52) and (53). The actual friction coefficient of approximately 2.0, which is obtained from an empirical measurement, ensures rolling during the experiment.

B. Balancing with Angular Velocity Control

In this experiment, the task of balancing the object is performed while the hand is simultaneously controlled to spin at an angular velocity of -4 rad/s.
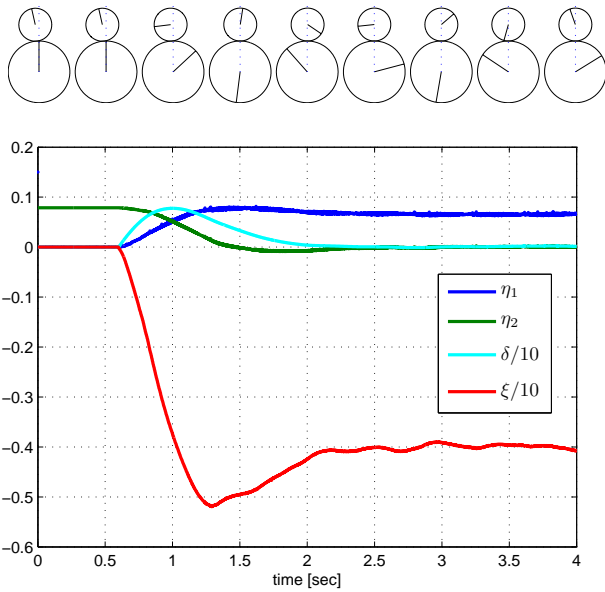
Fig. 12. Experimental result showing the state variables η_1, η_2, δ, and ξ for balancing with angular velocity control. The target angular velocity of the hand is -4 rad/s. The control action starts at $t = 0.60$ s. The icons at top show the configurations of the disks every 0.5 seconds.

Fig. 12 shows the state variables $(\eta_1, \eta_2, \delta, \xi)$. With the target hand velocity of -4 rad/s, the initial conditions were given as $(\eta_1, \eta_2, \delta, \xi) = (0, 0.0787, 0, 0)$. The control gains were chosen as $(k_1, k_2, k_3, k_4) = (16, 96, 256, 256)$ with the repeated root of the characteristic equation at -4. The control action started at $t = 0.60$. After ξ settles within ± 2 % of the target velocity, i.e., 0.08 rad/s, at $t = 2.12$ s, the RMS error of the hand velocity is 0.0513 rad/s and the RMS error of η_2 is 0.0016 ($0.092°$). The required friction coefficient to prevent slip during this experiment is computed to be greater than 0.08.

VII. CONCLUSIONS

In this paper, as a first step to understanding the nature of dynamic nonprehensile manipulation, we studied the canonical rolling manipulation problem of a disk rolling on a disk. We derived the kinematic and dynamic equations of the disk-on-disk system. Based on these, we derived and demonstrated controllers to balance the object disk at the unstable upright position while the hand or object rotates to a specific orientation or spins at a constant velocity. The importance of this work is that it is a concrete step toward establishing rolling as a viable manipulation primitive. The presented approach can possibly be extended in theory to complete the same tasks with non-symmetric objects like its center of mass is not on the geometric center, by considering the control task is to balance the object's center of mass on the vertical line at the contact point. Future work will focus on motion planning and feedback stabilization of a broad class of rolling trajectories for smooth planar objects rolling on smooth planar hands (other than disks) moving with a full three degrees-of-freedom.

The resulting dynamic rolling manipulation primitive will be incorporated into our library of nonprehensile manipulation primitives toward the development of a unified framework for planning and control of dynamic robotic manipulation.

REFERENCES

[1] K. M. Lynch and M. T. Mason, "Dynamic underactuated nonprehensile manipulation," in *Proc. IEEE/RSJ Int. Conf. on Intelligent Robots and Systems (IROS)*, 1996, pp. 889–896.
[2] ——, "Dynamic nonprehensile manipulation: Controllability, planning, and experiments," *Int. J. of Robotics Research*, vol. 18, no. 1, pp. 64–92, 1999.
[3] M. T. Mason, "Progress in nonprehensile manipulation," *Int. J. of Robotics Research*, vol. 18, no. 11, pp. 1129–1141, 1999.
[4] K. M. Lynch and T. D. Murphey, "Control of nonprehensile manipulation," in *Control Problems in Robotics and Automation*. Springer-Verlag, 2003, p. 39–58.
[5] K. M. Lynch, N. Shiroma, H. Arai, and K. Tanie, "The roles of shape and motion in dynamic manipulation: The butterfly example," in *Proc. IEEE Int. Conf. on Robotics and Automation*, 1998, pp. 1958–1963.
[6] J. Hauser, S. Sastry, and P. Kokotovic, "Nonlinear control via approximate input-output linearization: the ball and beam example," *IEEE Trans. on Automatic Control*, vol. 37, pp. 392–398, 1992.
[7] C. Barbu, R. Sepulchre, W. Lin, and P. V. Kokotovic, "Global asymptotic stabilization of the ball-and-beam system," in *Proc. IEEE Conf. on Decision and Control*, vol. 3, 1997, pp. 2351–2355.
[8] N. B. Almutairi and M. Zribi, "On the sliding mode control of a ball on a beam system," *Nonlinear Dynamics*, vol. 59, pp. 221–238, 2010.
[9] Z. Li and J. Canny, "Motion of two rigid bodies with rolling constraint," *IEEE Trans. on Robotics and Automation*, vol. 6, pp. 62–72, 1990.
[10] R. Mukherjee, M. A. Minor, and J. T. Pukrushpan, "Motion planning for a spherical mobile robot: Revisiting the classical ball-plate problem," *ASME Transactions, Journal of Dynamic Systems, Measurement, and Control*, vol. 124, pp. 502–511, 2002.
[11] A. Bicchi, A. Balluchi, D. P. tichizzo, and A. GoreUjt, "Introducing the sphericle: an experimental testbed for research and teaching in nonholonomy," in *Proc. IEEE Int. Conf. on Robotics and Automation*, vol. 3, 1997, pp. 2620–2625.
[12] S. Bhattacharya and S. K. Agrawal, "Spherical rolling robot: a design and motion planning studies," *IEEE Trans. on Robotics and Automation*, vol. 16, pp. 835–839, 2000.
[13] H. date, M. Sampei, M. Ishikawa, and M. Koga, "Simultaneous control of position and orientation for ball-plate manipulation problem based on time-state control form," *IEEE Trans. on Robotics and Automation*, vol. 20, pp. 465–479, 2004.
[14] G. Oriolo and M. Vendittelli, "A framework for the stabilization of general systems with an application to the plate-ball mechanism," *IEEE Transactions on Robotics*, vol. 21, pp. 162–175, 2005.
[15] S. Awtar, C. Bernard, N. Boklund, A. Master, D. Ueda, and K. Craig, "Mechatronic design of a ball-on-plate balancing system," *Mechatronics*, vol. 12, pp. 217–228, 2002.
[16] M. Cefalo, L. Lanari, and G. Oriolo, "Energy-based control of the butterfly robot," in *8th International IFAC Symposium on Robot Control*, vol. 8, 2006.
[17] J.-C. Ryu, F. Ruggiero, and K. M. Lynch, "Control of nonprehensile rolling manipulation: Balancing a disk on a disk," in *Proc. IEEE Int. Conf. on Robotics and Automation*, 2012, pp. 3232–3237.
[18] A. Isidori, *Nonlinear Control Systems*, 3rd ed. Springer, 1995.
[19] H. K. Khalil, *Nonlinear Systems*, 3rd ed. Prentice Hall, 2001.

Ji-Chul Ryu received his Ph.D degree in Mechanical Engineering from the University of Delaware in 2009 and his B.S and M.S degrees in Mechanical Engineering from Korea Advanced Institute of Science and Technology (KAIST). From 1999 to 2004, he worked as a research engineer at companies including Samsung, where he developed various types of automated robotic machines. Currently, he is a postdoctoral fellow in the Neuroscience and Robotics Laboratory at Northwestern University and is going to start as an assistant professor in the Department of Mechanical Engineering at Northern Illinois University in August 2013. He is a recipient of the MSC Simulation Software Award at ASME IDETC/CIE 2007 and a member of editorial board of the international journal of Advances in Robotics Research. His research interests include integrated planning and control of autonomous robotic systems, its application to mobility assistive robots, and dynamic robotic manipulations.

Fabio Ruggiero was born in Naples, Italy, on December 16, 1983. He received the Laurea Specialistica degree (M.Sc.) in Automation Engineering from the University of Naples in 2007. He got the Ph.D. degree from the same institution in 2010. Fabio Ruggiero has been holding a PostDoctoral position at Department of Electrical Engineering and Information Technology at University of Naples since 2011. His research interests are focused on dexterous and dual-hand robotic manipulation, even by using UAVs with small robotic arms, dynamic manipulation, 3D object preshaping and reconstruction. He has co-authored about twenty journal papers, book chapters and conference papers.

Kevin M. Lynch is Professor and Chair of Mechanical Engineering, and a member of the Neuroscience and Robotics Lab (NxR), in the McCormick School of Engineering and Applied Science at Northwestern University. His research focuses on robot manipulation and locomotion, self-organizing multi-agent systems, bio-inspired sensing and control, and functional electrical stimulation for restoration of human function. He is a Senior Editor of the IEEE Transactions on Automation Science and Engineering, co-author of "The Principles of Robot Motion" (MIT Press, 2005), a former member of the DARPA Defense Science Study Group, recipient of the 2001 IEEE Early Career Award in Robotics and Automation, the recipient of Northwestern's Professorship of Teaching Excellence and the engineering Teacher of the Year award, and an IEEE Fellow. He earned a BSE in Electrical Engineering from Princeton University and a PhD in Robotics from Carnegie Mellon University.